
MLRG Deep Curvature: An Open-source Package to Analyse and Visualise Neural Network Curvature and Loss Surface

Diego Granzio^{*1} Xingchen Wan^{*1} Timur Garipov²³ Dmitry Vetrov²³ Stephen Roberts¹

Abstract

We present MLRG Deep Curvature suite, a PyTorch-based, open-source package for analysis and visualisation of neural network curvature and loss landscape. Despite of providing rich information into properties of neural network and useful for a various designed tasks, curvature information is still not made sufficient use for various reasons, and our method aims to bridge this gap. We present a primer, including its main practical desiderata and common misconceptions, of *Lanczos algorithm*, the theoretical backbone of our package, and present a series of examples based on synthetic toy examples and realistic modern neural networks tested on CIFAR datasets, and show the superiority of our package against existing competing approaches for the similar purposes.

the curvature at a point in weight space, has not kept abreast. Researchers aspiring to evaluate or use curvature information need to implement their own libraries, which are rarely shared or kept up to date. Naive implementations are computationally intractable for all but the smallest of models. Hence, researchers typically either completely ignore curvature information or use highly optimistic approximations, such as the diagonal elements of the matrix or of a surrogate matrix, with limited justification or empirical analysis of the harshness of the aforementioned approximations.

Although the combination of fast Hessian vector products (Pearlmutter, 1994), advanced linear algebraic techniques (Golub & Meurant, 1994) and high dimensional geometry (Hutchinson, 1990) holds the key to solving to making significant process in this space, the lack of focus given to these areas, means that implementations of these methods (to the extent that they exist at all), are either inefficient or incorrect. In this paper we

1. Introduction

The success of deep learning models trained with gradient based optimizers on a range of tasks, from image classification/segmentation, natural language processing to reinforcement learning, often beating human level performance, has led to an explosion in the availability and ease of use of high performance software for their implementation. Automatic differentiation packages such as TensorFlow (Abadi et al., 2016) and PyTorch (Paszke et al., 2017) have become widely adopted, with higher level packages allowing users to state their model, dataset and optimiser in a few lines of code (Chollet, 2015), effortlessly achieving state of the art performance.

However, the pace of development of software packages extracting second order information, representing

- Motivate the use of curvature information, for both optimization, generalization, understanding the quality of optima, the effect of normalization techniques and evaluating theoretical assumptions
- Provide a primer on iterative methods, particularly the Lanczos algorithm, typical pitfalls and errors in its implementation and interpretation. We highlight its link to orthogonal polynomials, the problem of moments and how it can be used to generate a highly representative spectral approximation with minimal computational or memory overhead
- Provide a primer on typical matrix assumptions used for evaluating spectra in deep learning, such as the diagonal or diagonal generalised Gauss-Newton approximation and evaluate their efficacy on both small random matrices corresponding to known eigenvalue distributions and deep neural networks
- We provide an open-source PyTorch based software package, the **MLRG Deep Curvature** suite¹, which

^{*}Equal contribution ¹Machine Learning Research Group, University of Oxford. Correspondence to {diego, xwan}@robots.ox.ac.uk ²Samsung AI Centre, Moscow ³National Research University Higher School of Economics. Correspondence to: Diego Granzio <diego@robots.ox.ac.uk>.

¹Available at https://github.com/xingchenwan/MLRG_DeepCurvature

allows for spectral calculations on large expressive modern networks. We present examples of its usage on VGG networks (Simonyan & Zisserman, 2014) and Preactivated ResNets (He et al., 2016), with or without batch-normalization in a matter minutes on a single GPU.

- As a minor contribution, we also allow the calculation of various other useful quantities, such as the weight norm, gradient norm, variance of the gradient/hessian/loss along with an implementation of iterative stochastic newton methods for deep learning algorithms

2. Importance of Curvature in Deep Learning

The curvature at a point in weight-space informs us about the local conditioning of the problem, which determines the rate of convergence for first order methods and informs us about the optimal learning and momentum rates (Nesterov, 2013). The most common areas where curvature information is employed are analyses of the **Loss Surface** and **Newton** type methods in optimization.

2.1. Loss Surfaces

Loss surface visualization of deep neural networks, have often focused on two dimensional slices of random vectors (Li et al., 2017) or the changes in the loss traversing a set of random vectors drawn from the d -dimensional Gaussian distribution (Izmailov et al., 2018). Recent empirical analyses of the neural network loss surfaces invoking full eigen-decomposition (Sagun et al., 2016; 2017) have been limited to toy examples with 2-hidden layers and only some 5k parameters. Other works that have considered loss surface visualization have used the diagonal of the Fisher information matrix (Chaudhari et al., 2016), an assumption we will challenge in later sections of this paper. Theoretical analysis relating the loss surface to spin-glass models from condensed matter physics and associated random matrix theory (Choromanska et al., 2015b;a) rely on a number of unrealistic assumptions² and it is unclear to what extent the violation of such assumptions alters the theoretical results. Given that random matrices are known to have spectra which follow specific distributions in the asymptotic limit (Tao, 2012; Akemann et al., 2011), it may be helpful to better understand the spectra of large real networks and commonly used datasets to better and evaluate to what extent the observed spectra deviate from theoretical predictions and hence to what extent the underlying assumptions are violated. Other important areas of loss surface investigation include understanding the effectiveness of batch normalization (Ioffe & Szegedy, 2015). Recent convergence proofs

²such as input independence

(Santurkar et al., 2018) bound the maximal eigenvalue of the Hessian with respect to the activations and bounds with respect to the weights on a per layer basis. Bounds on a per layer basis do not imply anything about the bounds of the entire Hessian and furthermore it has been argued that the full spectrum must be calculated to give insights on the alteration of the landscape (Kohler et al., 2018).

2.2. Newton Methods in Deep Learning

In cases where the optimisation is plagued by locally dependent, tightly coupled parameters, or large variations in scale along different vectors in the parameter space, second-order methods can be expected to significantly outperform first order methods. Practical implementations, such as the Hessian free method (Martens, 2010; Dauphin et al., 2014; Vinyals & Povey, 2012), continue to be useful in a plethora of applications (Graff et al., 2014; Chung et al., 2017), requiring orders of magnitude fewer iterations than SGD. All second order methods solve the minimisation problem for the loss, L associated with parameters \mathbf{p} and perturbation \mathbf{d} to the second order in Taylor expansion,

$$\begin{aligned} \mathbf{d}^* &= \operatorname{argmin}_{\mathbf{d}} L(\mathbf{p} + \mathbf{d}) \\ L(\mathbf{p} + \mathbf{d}) &= L(\mathbf{p}) + \nabla L^T \mathbf{d} + \frac{1}{2} \mathbf{d}^T \bar{\mathbf{H}} \mathbf{d} \end{aligned} \quad (1)$$

Where instead of the true Hessian $\mathbf{H} \in \mathbb{R}^{n \times n} = \nabla \nabla L(\mathbf{p})$, a surrogate positive definite approximation to the Hessian $\bar{\mathbf{H}}$, such as the Gauss-Newton is employed so to make sure the minimum is lower bounded and its solution is

$$\mathbf{d} = -\bar{\mathbf{H}}^{-1} \nabla L(\mathbf{p}) = - \sum_i^N \frac{1}{\lambda_i} \mathbf{u}_i \mathbf{u}_i^T \nabla L(\mathbf{p}) \quad (2)$$

Where \mathbf{u}_i correspond to the generalised Hessian eigenvectors. The parameters are updated with $\mathbf{p} = \mathbf{p} - \alpha \mathbf{d}$. Where α is the global learning rate.

Despite the success of second order optimisation for difficult problems on which SGD is known to stall, such as recurrent neural networks (Martens & Sutskever, 2012), or auto-encoders (Martens, 2016). Researchers wanting to implement second order methods such as (Vinyals & Povey, 2012; Martens & Sutskever, 2012; Dauphin et al., 2014) face the aforementioned problems of difficult implementation. As a minor contribution, we also include two stochastic Lanczos based optimisers in our code, one which uses the absolute eigenvalues of the Hessian (Dauphin et al., 2014) and another which uses the Generalised-Gauss-Newton approximation, which is similar to the conjugate gradient method of (Martens & Sutskever, 2012).

Bayesian Neural Networks As a minor remark, we note that Bayesian neural networks use the Laplace approximation, featuring the inverse of the Hessian multiplied by a

Algorithm 1 Lanczos Algorithm

```

1: Input: Hessian vector product  $\{\mathbf{H}\mathbf{v}\}$ , number of steps
    $m$ 
2: Output: Ritz eigenvalue/eigenvector pairs  $\{\lambda_i, \mathbf{u}_i\}$  &
   quadrature weights  $\tau_i$ 
3:  $\mathbf{v} = \mathbf{v} / \sqrt{\mathbf{v}^T \mathbf{v}}$ 
4:  $\beta = 0$  &  $\mathbf{v}_{old} = \mathbf{v}$ 
5:  $\mathbf{V}(:, 1) = \mathbf{v}$ 
6: for  $j$  in  $1, \dots, m$  do
7:    $\mathbf{w} = \mathbf{H}\mathbf{v} - \beta \mathbf{v}_{old}$ 
8:    $\mathbf{T}(j, j) = \alpha = \mathbf{w}^T \mathbf{v}$ 
9:    $\mathbf{w} = \mathbf{w} - \alpha \mathbf{v} - \mathbf{V}\mathbf{V}^T \mathbf{w}$ 
10:   $\beta = \sqrt{\mathbf{w}^T \mathbf{w}}$ 
11:   $\mathbf{v}_{old} = \mathbf{v}$ 
12:   $\mathbf{v} = \mathbf{w} / \beta$ 
13:   $\mathbf{V}(:, j+1) = \mathbf{v}$ 
14:   $\mathbf{T}(j, j+1) = \mathbf{T}(j+1, j) = \beta$ 
15: end for
16:  $[\lambda_i, \mathbf{e}_i] = \text{eig}(\mathbf{T})$ 
17:  $\mathbf{u}_i = \mathbf{V}\mathbf{e}_i$ 
18:  $\tau_i = (\mathbf{e}_i^T [1, 0, \dots, 0])^2$ 

```

vector (Bishop, 2006). Our code allows for an estimation of this quantity, which may also be of use to the community and serve as an alternative for KFAC-Laplace.

3. Lanczos Algorithm

The Lanczos algorithm, has a rich history (Meurant & Strakoš, 2006; Golub & Meurant, 1994; Van Loan & Golub, 1983), with elegant proofs of convergence, error analysis for finite precision, relationships to Gauss-quadrature rules, orthogonal polynomials and the problem of moments. Given that Lanczos algorithm is one of the key theoretical foundations of our proposed tool and is often subjected to various misconceptions commonly seen in literature, we summarise some of its main properties here.

The Lanczos Algorithm (Algorithm 1) is an iterative algorithm for learning a subset of the eigenvalues/eigenvectors of any Hermitian matrix, requiring only matrix vector products. It can be regarded as an adaptation of the power iteration method, where the Krylov subspace $\mathcal{K}(\mathbf{H}, \mathbf{v}) = \text{span}\{\mathbf{v}, \mathbf{H}^2\mathbf{v}, \mathbf{H}^3\mathbf{v}, \dots\}$ is orthogonalised using Gram-Schmidt. Beyond having improved convergence to the power iteration method (Bai et al., 1996) by storing the intermediate orthogonal vectors in the corresponding Krylov subspace, Lanczos produces estimates of the eigenvectors and eigenvalues of smaller absolute magnitude, known as Ritz vectors/values.

3.1. Convergence Rate: Lanczos vs Power Iteration

The Lanczos method be be explicitly derived by considering the optimization of the Rayleigh quotient (Golub & Van Loan, 2012)

$$r(\mathbf{v}) = \frac{\mathbf{v}^T \mathbf{H} \mathbf{v}}{\mathbf{v}^T \mathbf{v}} \quad (3)$$

over the entire Krylov subspace $\mathcal{K}_m(\mathbf{H}, \mathbf{v})$ as opposed to power iteration which is a particular vector in the Krylov subspace $\mathbf{u} = \mathbf{H}^m \mathbf{v}$. This can be shown with the following convergence theorems

Theorem 1. Let $H^{P \times P}$ be a symmetric matrix with eigenvalues $\lambda_1 \geq \dots \geq \lambda_P$ and corresponding orthonormal eigenvectors $\mathbf{z}_1, \dots, \mathbf{z}_P$. If $\theta_1 \geq \dots \geq \theta_m$ are the eigenvalues of the matrix T_m obtained after m Lanczos steps and $\mathbf{q}_1, \dots, \mathbf{q}_m$ the corresponding Ritz eigenvectors then

$$\begin{aligned} \lambda_1 \geq \theta_1 &\geq \lambda_1 - \frac{(\lambda_1 - \lambda_n) \tan^2(\theta_1)}{(c_{m-1}(1 + 2\rho_1))^2} \\ \lambda_P \leq \theta_k &\leq \lambda_m + \frac{(\lambda_1 - \lambda_n) \tan^2(\theta_1)}{(c_{m-1}(1 + 2\rho_1))^2} \end{aligned} \quad (4)$$

where c_m is the Chebyshev polyomial of order k . $\cos \theta_1 = |\mathbf{q}_1^T \mathbf{z}_1|$ & $\rho_1 = (\lambda_1 - \lambda_2)/(\lambda_2 - \lambda_n)$

Proof. see (Golub & Van Loan, 2012). \square

Theorem 2. Assuming the same notation as in Theorem 1, after m power iteration steps the corresponding extremal eigenvalue estimate is lower bounded by

$$\lambda_1 \geq \theta_1 \geq \lambda_1 - (\lambda_1 - \lambda_n) \tan^2(\theta_1) \left(\frac{\lambda_2}{\lambda_1} \right)^{2m-1} \quad (5)$$

From the rapid growth of orthogonal polynomials such as Chebyshev, we expect Lanczos superiority to significantly emerge for larger spectral gap and iteration number. To verify this experimentally, we collect the non identical terms in the equations 4 and 5 of the lower bounds for λ_1 derived by Lanczos and Power iteration and denote them L_{k-1} and R_{k-1} respectively. For different values of λ_1/λ_2 and iteration number m we give the ratio of these two quantities in Table 1. As can be clearly seen, the Lanczos lower bound is always closer to the true value, this improves with the iteration number m and its relative edge is reduced if the spectral gap is decreased.

3.2. The Problem of Moments: Spectral Density Estimation Using Lanczos

In this section we show that that the Lanczos Tri-Diagonal matrix corresponds to an orthogonal polynomial basis which matches the moments of $\mathbf{v}^T \mathbf{H}^m \mathbf{v}$ and that when \mathbf{v} is a zero mean random vector with unit variance, this corresponds to the moment of the underlying spectral density.

λ_1/λ_2	$m = 5$	$m = 10$	$m = 15$	$m = 20$
1.5	1.1×10^{-4} 3.9×10^{-2}	2×10^{-10} 6.8×10^{-4}	3.9×10^{-16} 1.2×10^{-5}	7.4×10^{-22} 2.0×10^{-7}
1.1	2.7×10^{-2} 4.7×10^{-1}	5.5×10^{-5} 1.8×10^{-1}	1.1×10^{-7} 6.9×10^{-2}	2.1×10^{-10} 2.7×10^{-2}
1.01	5.6×10^{-1} 9.2×10^{-1}	1.0×10^{-1} 8.4×10^{-1}	1.5×10^{-2} 7.6×10^{-1}	2.0×10^{-3} 6.9×10^{-1}

Table 1. L_{k-1}/R_{k-1} For different values of spectral gap λ_1/λ_2 and iteration number m , Table from (Golub & Van Loan, 2012)

Stochastic trace estimation Using the expectation of quadratic forms, for zero mean, unit variance random vectors

$$\begin{aligned} \mathbb{E}_v \text{Tr}(\mathbf{v}^T \mathbf{H}^m \mathbf{v}) &= \text{Tr} \mathbb{E}_v(\mathbf{v} \mathbf{v}^T \mathbf{H}^m) = \text{Tr}(\mathbf{H}^m) \\ &= \sum_{i=1}^P \lambda_i^m = P \int_{\lambda \in \mathcal{D}} \lambda^m d\mu(\lambda) \end{aligned} \quad (6)$$

where we have used the linearity of trace and expectation. Hence in expectation over the set of random vectors, the trace of the inner product of \mathbf{v} and $\mathbf{H}^m \mathbf{v}$ is equal to the m 'th moment of the spectral density of \mathbf{H} .

Lanczos-Stieltjes The Lanczos tri-diagonal matrix \mathbf{T} can be derived from the Moment matrix \mathbf{M} , corresponding to the discrete measure $d\alpha(\lambda)$ satisfying the moments $\mu_i = \mathbf{v}^T \mathbf{H}^i \mathbf{v} = \int \lambda^i d\alpha(\lambda)$ (Golub & Meurant, 1994)

$$\mathbf{M} = \begin{bmatrix} 1 & \mathbf{v}^T \mathbf{H} \mathbf{v} & \dots & \mathbf{v}^T \mathbf{H}^{m-1} \mathbf{v} \\ \mathbf{v}^T \mathbf{H} \mathbf{v} & \mathbf{v}^T \mathbf{H}^2 \mathbf{v} & \ddots & \vdots \\ \vdots & \ddots & \ddots & \vdots \\ \mathbf{v}^T \mathbf{H}^{m-1} \mathbf{v} & \dots & \dots & \mathbf{v}^T \mathbf{H}^{2m-2} \mathbf{v} \end{bmatrix}$$

and hence for a zero mean unit variance initial seed vector, the eigenvector/eigenvalue pairs of \mathbf{T} contain information about the spectral density of \mathbf{H} as shown in section 3.2. This is given by the following Theorem

Theorem 3. *The eigenvalues of T_k are the nodes t_j of the Gauss quadrature rule, the weights w_j are the squares of the first elements of the normalized eigenvectors of T_k*

Proof. See (Golub & Meurant, 1994) \square

A quadrature rule is a relation of the form,

$$\int_a^b f(\lambda) d\mu(\lambda) = \sum_{j=1}^M \rho_j f(t_j) + R[f] \quad (7)$$

for a function f , such that its Riemann-Stieltjes integral and all the moments exist on the measure $d\mu(\lambda)$, on the interval $[a, b]$ and where $R[f]$ denotes the unknown remainder. The first term on the RHS of equation 7 using Theorem 3 can be seen as a discrete approximation to the spectral density

matching the first m moments $\mathbf{v}^T \mathbf{H}^m \mathbf{v}$ (Golub & Meurant, 1994; Golub & Van Loan, 2012)

For n_v starting vectors, the corresponding discrete spectral density is given as

$$p(\lambda) = \frac{1}{n_v} \sum_{l=1}^{n_v} \left(\sum_{k=1}^m (\tau_k^{(l)})^2 \delta(\lambda - \lambda_k^{(l)}) \right), \quad (8)$$

where $\tau_k^{(l)}$ corresponds to the first entry of the eigenvector of the k -th eigenvalue, λ_k , of the Lanczos tri-diagonal matrix, \mathbf{T} , for the l -th starting vector (Ubaru & Saad; Lin et al., 2016).

Number of trace vectors used The error between the expectation over the set of all zero mean, unit variance vectors \mathbf{v} and the monte carlo sum used in practice can be bounded (Hutchinson, 1990; Roosta-Khorasani & Ascher, 2015). However these bounds are very loose, with typical matrices requiring hundreds of thousands of random vectors to guarantee a reasonable guarantee on fractional error (Granzio et al., 2018b) with authors typically using a vastly reduced number of random vectors in practice (Granzio et al., 2019; 2018b;a; Granzio & Roberts, 2017; Papyan, 2018; Ghorbani et al., 2019).

Importance of keeping orthogonality The update equations of the Lanczos algorithm lead to a tri-diagonal matrix $\mathbf{T} = \mathbb{R}^{m \times m}$, whose eigenvalues represent the approximated eigenvalues of the matrix \mathbf{H} and whose eigenvectors, when projected back into the Krylov-subspace, $\mathcal{K}(\mathbf{H}, \mathbf{v})$, give the approximated eigenvectors of \mathbf{H} . In finite precision, it is known (Meurant & Strakoš, 2006) that the Lanczos algorithm fails to maintain orthogonality between its Ritz vectors, with corresponding convergence failure. In order to remedy this, we re-orthonormalise at each step (Bai et al., 1996) (as shown in line 9 of Algorithm 1) and observe a high degree of orthonormality between the Ritz eigenvectors. Orthonormality is also essential for achieving accurate spectral resolution as the Ritz value weights are given by the squares of the first elements of the normalised eigenvectors. For the practitioner wishing to reduce the computational cost of maintaining orthogonality, there exist more elaborate schemes (Meurant & Strakoš, 2006; Golub & Meurant, 1994).

3.3. Computational Complexity

For large matrices, the computational complexity of the algorithm depends on the Hessian vector product, which for neural networks is $\mathcal{O}(mNP)$ where P denotes the number of parameters in the network, m is the number of Lanczos iterations and N is the number of data-points. The full re-orthogonalisation adds two matrix vector products, which is of cost $\mathcal{O}(m^2P)$, where typically $m^2 \ll N$. Each random

vector used can be seen as another full run of the Lanczos algorithm, so for d random vectors the total complexity is $\mathcal{O}(dmP(N+m))$

3.4. Debunking Common Myths in the Literature

Due to its involved mathematical nature relative to its simpler power iteration counterpart, the Lanczos algorithm, as applied use in machine learning, is unfortunately subjected a range of misconceptions and misuse. Because the our software package relies strongly on the Lanczos algorithm, as we advocate for broader usage of Lanczos, we feel it is imperative to state some of the common misconceptions to avoid potential misinterpretations of our results, and results from Lanczos algorithm in general. Here, we highlight two most common misconceptions:

- We can learn the negative and interior eigenvalues by shifting and inverting the matrix sign $\mathbf{H} \rightarrow -\mathbf{H} + \mu\mathbf{I}$
- Lanczos learns the largest m $[\lambda_i, \mathbf{u}_i]$ pairs of $\mathbf{H} \in \mathbb{R}^{P \times P}$ with high probability (Dauphin et al., 2014)

Since these two related beliefs are prevalent, we disprove them explicitly in this section, with Theorems 4 and 5.

Theorem 4. *The shift and invert procedure $\mathbf{H} \rightarrow -\mathbf{H} + \mu\mathbf{I}$, changes the Eigenvalues of the Tri-diagonal matrix \mathbf{T} (and hence the Ritz values) to $\lambda_i = -\lambda_i + \mu$*

Proof. Following the equations from Algorithm 1

$$\begin{aligned} \mathbf{w}_1^T &= (-\mathbf{H} + \mu\mathbf{I})\mathbf{v}_1 \ \& \alpha_1 = \mathbf{v}_1^T \mathbf{H} \mathbf{v}_1 + \mu \\ \mathbf{w}_2 &= \mathbf{w}_1 - \alpha_1 \mathbf{v}_1 = (\mathbf{H} + \mu\mathbf{I})\mathbf{v}_1 - (\mathbf{v}_1^T \mathbf{H} \mathbf{v}_1 + \mu)\mathbf{v}_1 \\ \mathbf{w}_2 &= (\mathbf{H} - \mathbf{v}_1^T \mathbf{H} \mathbf{v}_1)\mathbf{v}_1 \ \& \ \mathbf{v}_2 = \mathbf{w}_2 / \|\mathbf{w}_2\| \\ \alpha_2 &= \mathbf{v}_2^T (-\mathbf{H} + \mu\mathbf{I})\mathbf{v}_2 = -\mathbf{v}_2^T \mathbf{H} \mathbf{v}_2 + \mu \\ \beta_2 &= \|\mathbf{w}_2\| \end{aligned} \quad (9)$$

assuming for $m-1$ and repeating the above steps for m we prove by induction and finally arrive at the modified Tridiagonal Lanczos matrix $\tilde{\mathbf{T}}$

$$\begin{aligned} \tilde{\mathbf{T}} &= -\mathbf{T} + \mu\mathbf{I} \\ \tilde{\lambda}_i &= -\lambda_i + \mu \ \forall 1 \leq i \leq m \end{aligned} \quad (10)$$

□

Remark. hence no new Eigenvalues of the matrix \mathbf{H} are learned. Although it is obvious that the addition of the identity does not change the Krylov subspace, such procedures are common place in code pertaining to papers attempting to find the *smallest eigenvalue*. This disproves the first myth.

Theorem 5. *For any matrix $\mathbf{H} \in \mathbb{R}^{P \times P}$ such that $\lambda_1 > \lambda_2 \dots > \lambda_P$ and $\sum_{i=1}^m \lambda_i < \sum_{i=m+1}^P \lambda_i$ in expectation*

over the set of random vectors \mathbf{v} the m eigenvalues of the Lanczos Tridiagonal matrix \mathbf{T} do not correspond to the top m eigenvalues of \mathbf{H}

Proof. Let us consider the matrix $\tilde{\mathbf{H}} = \mathbf{H} - \frac{\lambda_{m+1} + \lambda_m}{2} \mathbf{I}$.

$$\begin{cases} \lambda_i > 0, & \forall i \leq m \\ \lambda_i < 0, & \forall i > m \end{cases} \quad (11)$$

Under the assumptions of the theorem, $\text{Tr}(\tilde{\mathbf{H}}) < 0$ and hence by Theorem 3 and equation 6 there exist no $w_i > 0$ such that

$$\sum_{i=1}^m w_i \lambda_i^k = \frac{1}{P} \sum_{i=1}^P \lambda_i^k \ \forall \ 1 \leq k \leq m \quad (12)$$

is satisfied for $k=1$ As the L.H.S is manifestly positive and the R.H.S is negative. By Theorem 4 this holds for the original matrix \mathbf{H} . □

Remark. Given that Theorem 5 is satisfied over the expectation of the set of random vectors, which by the CLT is realised by monte carlo draws of random vectors as $d \rightarrow \infty$ the only way to really span the top m eigenvectors is to have selected a vector which lies in the m dimensional subspace of the P dimensional problem corresponding to those vectors, which would correspond to knowing those vectors a priori, defeating the point of using Lanczos at all.

Another way to see this is Theorem 1, which gives a bound on the distance between the smallest Lanczos Ritz value and the minimal eigenvalue. Intuitively, as the Ritz values and weights form a discrete m -moment spectral approximation to the Hessian spectrum, hence the support of the discrete density, cannot approximately match the largest m eigenvalues. This can be seen in Figure 1c where we run Lanczos with $m=30$ steps and capture the shape of the spectral density of a $\mathbf{H} \in \mathbb{R}^{10000 \times 10000}$ matrix including the negative eigenvalue of largest magnitude.

4. MLRG Deep Curvature

Based on the Lanczos algorithm, we are in a position to introduce to our package, the **MLRG Deep Curvature suite**, a software package that allows analysis and visualisation of deep neural network curvature. The main features and functionalities of our package are:

- **Network training and evaluation** we provide a range of pre-built modern popular neural network structures, such as VGG and variants of ResNets, and various optimisation schemes in addition to the ones already present in the PyTorch frameworks, such as K-FAC and SWATS. These facilitates faster training and evaluation

of the networks (although it is worth noting that any PyTorch-compatible optimisers or architectures can be easily integrated into our analysis framework).

- **Eigenspectrum analysis of the curvature matrices** Powered by the Lanczos techniques outlined in Section 3, *with a single random vector* we use Pearlmutter matrix-vector product trick for fast computation for inference of the eigenvalues and eigenvectors of the common curvature matrices of the deep neural networks. In addition to the standard Hessian matrix, we also include the feature for inference of the eigen-information of the Generalised Gauss-Newton matrix, a commonly used positive-definite surrogate to Hessian³.
- **Advanced Statistics of Networks** In addition to the commonly used statistics to evaluate network training and performance such as the training and testing losses and accuracy, we support computations of more advanced statistics: For example, we support squared mean and variance of gradients and Hessians (and GGN), squared norms of Hessian and GGN, L2 and L-inf norms of the network weights and etc. These statistics are useful and relevant for a wide range of purposes such as the designs of second-order optimisers and network architecture.
- **Visualisations** For all main features above, we include accompanying visualisation tools. In addition, with the eigen-information obtained, we also feature visualisations of the **loss landscape** by studying the sensitivity of the neural network to perturbations of weights. While similar tools have been available, we would like to emphasise that one key difference is that, instead of the *random* directions as featured in some other packages, we explicitly perturb the weights in the *eigenvector* directions, which should yield more informative results.

Package Structure The main interface functions are organised as followed:

- **/core** The functions under `core` directories are the main analysis tools of the package. `train_network` allows network training and saving of the required statistics for subsequent spectrum learning. Based on the output of it, we additionally include tools for spectrum analysis (`compute_eigenspectrum`)

³The computation of the GGN-vector product is similar with the computational cost of two backward passes in the network. Also, GGN uses *forward-mode automatic differentiation* (FMAD) in addition to the commonly employed *backward-mode automatic differentiation* (RMAD). In the current PyTorch framework, the FMAD operation can be achieved using two equivalent RMAD operations.

and advanced loss statistics (such as covariance of gradients and second order information like Hessian variance) in `compute_loss_stats` and `build_loss_landscape`.

We provide some pre-built network architectures (such as VGG and ResNet architectures) and optimizers apart from PyTorch natives (such as K-FAC, SWATS optimizers). We additionally support Stochastic Weight Averaging proposed in (Izmailov et al., 2018). However, it is worth noting that any PyTorch compatible networks and optimizers can be easily integrated in our framework.

- **/visualise** This directory defines the various pre-defined visualisation functions for different purposes, including the visualisation of training, spectrum and the loss landscape.

To facilitate a quick start of our package, we have included an illustrated example of analysis on the VGG-16 network on CIFAR-100 dataset in Appendix A.

5. Examples on Small Random Matrices

In this section, we use some examples on small random matrices to showcase the power of our package that uses the Lanczos algorithm with random vectors to learn the spectral density. Here, we look at known random matrices with elements drawn from specific distributions which converge to known spectral densities in the asymptotic limit. Here we consider **Wigner Ensemble** (Wigner, 1993) and the **Marcenko Pastur** (Marchenko & Pastur, 1967), both of which are extensively used in simulations or theoretical analyses of deep neural network spectra (Pennington & Bahri, 2017; Choromanska et al., 2015a; Anonymous, 2020b).

5.1. Wigner Matrices

Wigner matrices can be defined in Definition 5.1, and their distributions of eigenvalues are governed by the semi-circle distribution law (Theorem 6).

Definition 5.1. Let $\{Y_i\}$ and $\{Z_{ij}\}_{1 \leq i \leq j}$ be two real-valued families of zero mean, i.i.d random variables, Furthermore suppose that $\mathbb{E}Z_{12}^2 = 1$ and for each $k \in \mathbb{N}$

$$\max(E|Z_{12}^k, E|Y_1|^k) < \infty \quad (13)$$

Consider a $P \times P$ symmetric matrix M_P , whose entries are given by

$$\begin{cases} M_P(i, i) = Y_i \\ M_P(i, j) = Z_{ij} = M_P(j, i), \quad \text{if } i \neq j \end{cases} \quad (14)$$

The Matrix M_P is known as a real symmetric Wigner matrix.

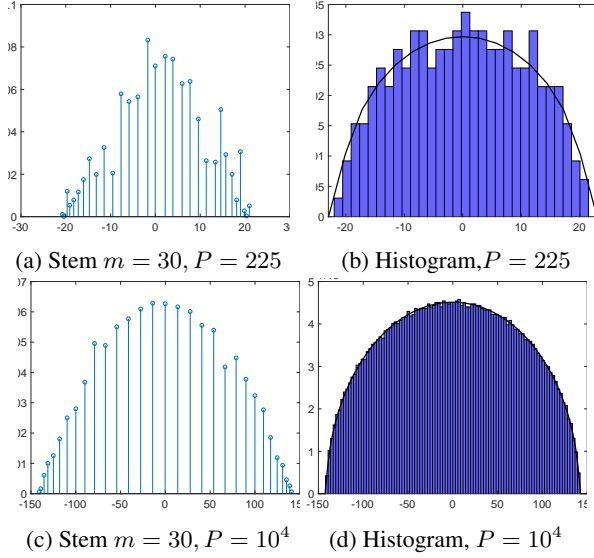


Figure 1. Lanczos stem plot for a single random vector with $m = 30$ steps compared to actual eigenvalue histogram for matrices of the form $\mathbf{H} \in \mathbb{R}^{P \times P}$, where each element is a drawn from a normal distribution with unit variance, converging to the Wigner semi circle.

Theorem 6. Let $\{M_P\}_{P=1}^{\infty}$ be a sequence of Wigner matrices, and for each P denote $X_P = M_P/\sqrt{P}$. Then μ_{X_P} , converges weakly, almost surely to the semi circle distribution,

$$\sigma(x)dx = \frac{1}{2\pi} \sqrt{4 - x^2} \mathbf{1}_{|x| \leq 2} \quad (15)$$

For our experiments, we generate random matrices $\mathbf{H} \in \mathbb{R}^{P \times P}$ with elements drawn from the distribution $\mathcal{N}(0, 1)$ for $P = \{225, 10000\}$ and plot histogram of the spectra found by eigendecomposition, along with the predicted Wigner density in Figures 1b & 1d and compare them along with the discrete spectral density approximation learned by lanczos in $m = 30$ steps using a single random vector $d = 1$ in Figures 1a & 1c. It can be seen that even for a small number of steps $m \ll P$ and a single random vector, Lanczos impressively captures not only the support of the eigenvalue spectral density but also its shape. We note as discussed in section 3.4 that the 30 Ritz values here do not span the top 30 eigenvalues even approximately.

5.2. Marcenko-Pastur

An equally important limiting law for the limiting spectral density of many classes of matrices constrained to be positive definite, such as the covariance matrices, is the Marcenko-Pastur law (Marchenko & Pastur, 1967). Formally, given a matrix $\mathbf{X} \in \mathbb{R}^{P \times T}$ with i.i.d zero mean entries with variance $\sigma^2 < \infty$. Let $\lambda_1 \geq \lambda_2, \dots \geq \lambda_P$ be eigenvalues of $\mathbf{Y}_n = \frac{1}{T} \mathbf{X} \mathbf{X}^T$. The random measure $\mu_P(A) = \frac{1}{P} \#\{\lambda_j \in A\}$, $A \in \mathbb{R}$

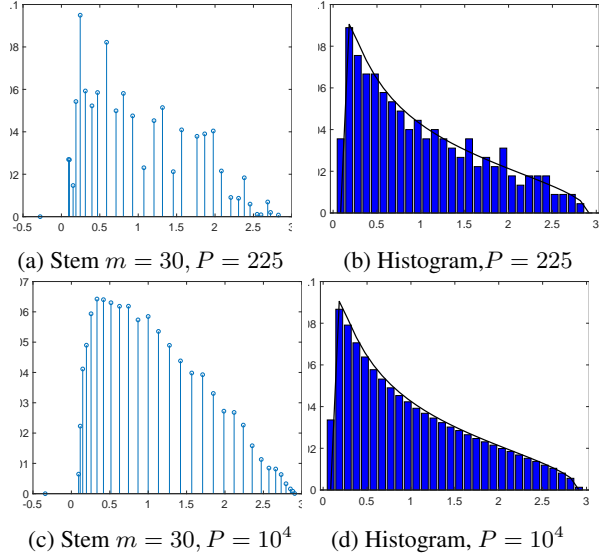


Figure 2. Lanczos stem plot for a single random vector with $m = 30$ steps compared to actual eigenvalue histogram for matrices of the form $\mathbf{H} \in \mathbb{R}^{P \times P}$, where $\mathbf{H} = \mathbf{X} \mathbf{X}^T/k$, where each element of $\mathbf{X}^{P \times k}$, $k = 2P$ is a drawn from a normal distribution with unit variance, converging to the Marcenko-Pastur distribution with $q = 2$.

Theorem 7. Assume that $P, N \rightarrow \infty$ and the ratio $P/N \rightarrow q \in (0, \infty)$ (this is known as the Kolmogorov limit) then $\mu_P \rightarrow \mu$ in distribution where

$$\begin{cases} (1 - \frac{1}{q}) \mathbb{1}_{0 \in A} + \nu_{1/q}(A), & \text{if } q > 1 \\ \nu_q(A), & \text{if } 0 \leq q \leq 1 \end{cases} \quad (16)$$

$$d\nu_q = \frac{1}{2\pi\sigma^2} \frac{\sqrt{(\lambda_+ - x)(x - \lambda_-)}}{\lambda x} \quad (17)$$

$$\lambda_{\pm} = \sigma^2(1 \pm \sqrt{q})^2$$

Here, we construct a random matrix $\mathbf{X} \in \mathbb{P} \times \mathbb{T}$ with independently drawn elements from the distribution $\mathcal{N}(0, 1)$ and then form the matrix $\frac{1}{T} \mathbf{X} \mathbf{X}^T$, which is known to converge to the Marcenko Pastur distribution. We use $P = \{225, 10000\}$ and $T = 2P$ and plot the associated histograms from full eigendecomposition in Figures 2b & 2d along with their $m = 30, d = 1$ Lanczos stem counterparts in Figures 2a & 2c. Similarly we see a faithful capturing not just of the support, but also of the general shape. We note that both for Figure 1 and Figure 2, the smoothness of the discrete spectral density for a single random vector increases significantly, even relative to the histogram. We also run the same experiment for $P = 10000$ but this time with $T = 0.5P$ so that exactly half of the eigenvalues will be 0. We compare the Histogram of the eigenvalues in Figure 3b against its $m = 30, d = 1$ Lanczos stem plot in Figure 3a and find both the density at the origin, along with the bulk and support to be faithfully captured.

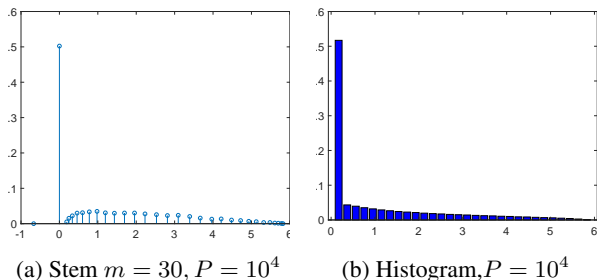


Figure 3. Lanczos stem plot for a single random vector with $m = 30$ steps compared to actual eigenvalue histogram for matrices of the form $\mathbf{H} \in \mathbb{R}^{P \times P}$, where $\mathbf{H} = \mathbf{X}\mathbf{X}^T/k$, where each element of $\mathbf{X}^{P \times k}$, $k = 0.5P$ is a drawn from a normal distribution with unit variance, converging to the Marcenko-Pastur distribution with $q = 0.5$.

As a proxy for deep neural network spectra, often the diagonal of the matrix (Bishop, 2006) or the diagonal of a surrogate matrix, such as the Fisher information, or that implied by the values of the Adam Optimizer (Chaudhari et al., 2016) is used. We plot the true eigenvalue estimates for random matrices pertaining to both the Marcenko-Pastur 4a and the Wigner density 4b in blue, along with the Lanczos estimate in red and the diagonal approximation in yellow. We see here that the diagonal approximation in both cases, fails to adequately the support or accurately model the spectral density, whereas the lanczos estimate is nearly indistinguishable from the true binned eigen-spectrum. This is of-course obvious from the mathematics of the un-normalised Wigner matrix. The diagonal elements are simply draws from the normal distribution $\mathcal{N}(0, 1)$ and so we expect the diagonal histogram plot to approximately follow this distribution (with variance 1). However the second moment of the Wigner Matrix can be given by the Frobenius norm identity

$$\mathbb{E}\left(\frac{1}{P} \sum_i \lambda_i^2\right) = \mathbb{E}\left(\frac{1}{P} \sum_{i,j=1}^P \mathbf{H}_{i,j}^2\right) = \mathbb{E}\left(\frac{1}{P} \chi_{P^2}^2\right) = P \quad (18)$$

Similarly for the Marcenko-Pastur distribution, We can easily see that each element of \mathbf{H} follows a chi-square distribution of $1/T\chi_T^2$, with mean 1 and variance $2/T$.

5.3. Synthetic Example

Curvature eigenspectrum of neural network often features a large spike at zero, a right-skewed bulk and some outliers (Sagun et al., 2016; 2017)⁴ In order to simulate the spectrum of a neural network, we generate a Matrix $\mathbf{H} \in \mathbb{R}^{1000 \times 1000}$ with 470 eigenvalues drawn from the uniform distribution from $[0, 15]$, 20 drawn from the uniform $[0, 60]$ and 10 drawn from the uniform $[-10, 0]$. The matrix is rotated

⁴Some examples of it can be found in later sections on real-life neural network experiments - see Figures 6 and 7.

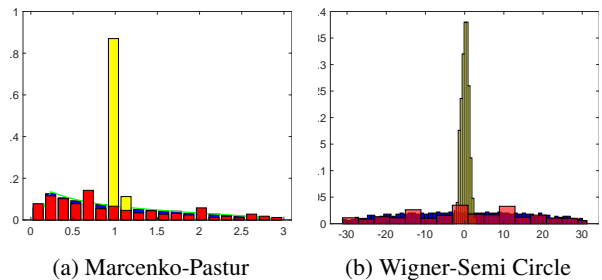


Figure 4. Two randomly generated matrices $\mathbf{H} \in \mathbb{R}^{500 \times 500}$ with the histogram of the true eigenvalues in blue, the Lanczos estimate $m = 30$, $d = 1$ in red and the diagonal approximation in yellow

through a rotation matrix U , i.e $\mathbf{H} = \mathbf{U}\mathbf{D}\mathbf{U}^T$ where \mathbf{D} is the diagonal matrix consisting of the eigenvalues and the columns are gaussian random vectors which are orthogonalised using Gram-Schmidt orthogonalisation. The resulting eigenspectrum is given in a histogram in Figure 5a and then using the same random vector, successive Lanczos stem plots for different number of iterations $m = [5, 30]$ are shown in Figure 5. Figure 5b, for a low number of steps, the degeneracy at $\lambda = 0$ is learned, as are the largest and smallest eigenvalues, some information is retained about the bulk density, but some of the outlier eigenvalues around $\lambda \approx 20$ and $\lambda \approx 30$ are completely missed out, along with all the negative outliers except the largest. For $m = 30$ even the shape of the bulk is accurately represented, as shown in Figure 5d. We note that the diagonal estimate in Figure 5c gives absolutely no spectral information, with no outliers shown (maximal and minimal diagonal elements being 5.3 and 3.3 respectively and it also gets the spectral mass at 0 wrong. This builds on section 5.2, as furthering the case against making diagonal approximations in general. In neural networks, the diagonal approximation is similar to positing no correlations between the weights. This is a very harsh assumption and usually a more reasonable assumption is to posit that the correlations between weights in the same layer are larger than between different layers, leading to a block diagonal approximation (Martens, 2016), however often when the layers have millions of parameters, full diagonal approximations are still used (Bishop, 2006; Chaudhari et al., 2016).

6. Neural Networks Examples

We showcase our spectral learning algorithm and visualization tool on real networks trained on real data-sets and we test on VGG networks (Simonyan & Zisserman, 2014). We train our neural networks using stochastic gradient descent with momentum $\rho = 0.9$, using a linearly decaying learning rate schedule. The learning rate at the t -th epoch is given

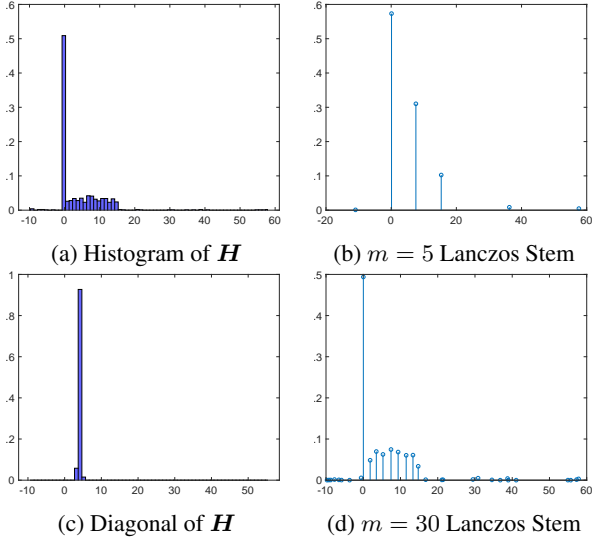


Figure 5. Generated matrices $\mathbf{H} \in \mathbb{R}^{1000 \times 1000}$ with known eigen-spectrum and Lanczos stem plots for different values of $m = \{5, 15, 30\}$

by:

$$\alpha_t = \begin{cases} \alpha_0, & \text{if } \frac{t}{T} \leq 0.5 \\ \alpha_0 \left[1 - \frac{(1-r)(\frac{t}{T} - 0.5)}{0.4} \right], & \text{if } 0.5 < \frac{t}{T} \leq 0.9 \\ \alpha_0 r, & \text{otherwise} \end{cases} \quad (19)$$

where α_0 is the initial learning rate. $T = 300$ is the total number of epochs budgeted for all experiments. We set $r = 0.01$. In our interface, to train the network, we call:

```
train_network (
  dir='result/VGG16-CIFAR100/',
  dataset='CIFAR100',
  # dataset='CIFAR10', if testing on
  # CIFAR-10 data-set.
  data_path='data/'
  data_path='data/',
  epochs=300,
  model='VGG16'
  # model='PreResNet110', if training
  # with Preactivated ResNet with 110
  # layers instead.
  optimizer='SGD',
  schedule='linear',
  # This will direct the learning rate
  # schedule to be the linear schedule
  # defined in Equation 19.
  optimizer_kwargs={
    'lr': 0.05,
    'momentum': 0.9,
    'weight_decay': 5e-4
  }
)
```

We compare our method against recently developed open-source tools which calculate on the fly diagonal Hessian

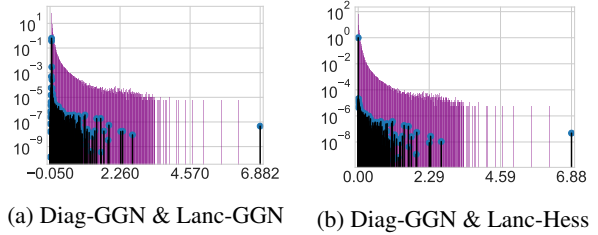


Figure 6. Diagonal Generalised Gauss Newton monte carlo approximation (Diag-GGN) against $m = 100$ Lanczos using Gauss-Newton vector products (Lanc-GGN) or Hessian vector products (Lanc-Hess)

and Generalised Gauss-Newton diagonal approximations (Anonymous, 2020a).

6.1. VGG-16

CIFAR-100 DATASET

We train a 16-layer VGG network, comprising of $P = 15, 291, 300$ parameters on the CIFAR-100 dataset, using $\alpha_0 = 1$. Even for this relatively small model, the open-source Hessian and GGN exact diagonal computations require over 125GB of GPU memory and so to avoid re-implementing the library to support multiple GPUs and node communication we use the Monte Carlo approximation to the GGN diagonal against both our GGN-Lanczos and Hessian-Lanczos spectral visualizations. We plot a histogram of the Monte Carlo approximation of the diagonal GGN (Diag-GGN) against both the Lanczos GGN (Lanc-GGN) and Lanczos Hessian (Lanc-Hess) in Figure 6. Note that as the Lanc-GGN and Lanc-Hess are displayed as stem plots (with the discrete spectral density summing to 1 as opposed to the histogram area summing to 1).

We note that the Gauss-Newton approximation quite closely resembles its Hessian counterpart, capturing the majority of the bulk and the outlier eigenvectors at $\lambda_1 \approx 6.88$ and the triad near $\lambda_i \approx 2.29$. The Hessian does still have significant spectral mass on the negative axis, around 37%. However most of this is captured by a Ritz value at -0.0003 , with this removed, the negative spectral mass is only 0.05%. However as expected from our previous section, the Diag-GGN gives a very poor spectral approximation. It vastly overestimates the bulk region, which extends well beyond $\lambda \approx 1$ implied by Lanczos and adds many spurious outliers between 3 and the misses the largest outlier of 6.88. To replicate this example, use the following command:

```
compute_eigenspectrum (
  dataset='CIFAR100',
  # dataset='CIFAR10', if testing on
  # CIFAR-10 data-set.
  data_path='data/'
)
```

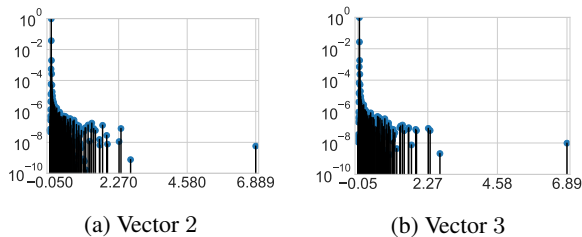


Figure 7. VGG16 Epoch 300 end of training Lanczos stem plot for different random vectors

```

data_path='data/',
model='VGG16',
checkpoint_path='result/VGG16-CIFAR100/
checkpoint-00300.pt',
save_spectrum_path='result/VGG16-
CIFAR100/spectra/spectrum-00300-
ggn_lanczos',
# change accordingly, if considering
the Hessian matrix
save_eigvec=True,
lanczos_iters=100,
curvature_matrix='ggn_lanczos',
# curvature_matrix='hessian_lanczos',
if considering the Hessian
instead
)

```

Effect of Varying Random Vectors Given that the proofs for the moments of Lanczos matching those of the underlying spectral density, are true over the expectation over the set of random vectors and in practice we only use a Monte Carlo average of random vectors, or in our experiments using stem plots, just a single random vector, it is prudent to at least consider experimentally how using different random vectors affect the resulting spectra. We hence run the same spectral visualisation as in Section 6.1 but using two different random vectors. We plot the results in Figure 7. We find both Figures 7a & 7b to be close to visually indistinguishable. There are minimal differences in the extremal eigenvalues, with former giving $\{\lambda_1, \lambda_n\} = \{6.8885, -0.0455\}$ and the latter $\{6.8891, -0.0456\}$, but the degeneracy at 0, bulk, triplet of outliers at 2.27 and the large outlier at 6.89 is unchanged.

Computational Cost Using a single NVIDIA GeForce GTX 1080 Ti GPU, the Gauss-Newton takes an average 26.5 seconds for each Lanczos iteration with the memory usage 2850Mb. Using the Hessian takes an average of 27.9 seconds for each Lanczos iteration with 2450Mb memory usage.

Local loss landscape The Lanczos algorithm with enforced orthogonality initialised with a random vector gives a moment matched discrete approximation to the Hessian

spectrum. However this information is local to the point in weight space w and the quadratic approximation may break down within the near vicinity. To investigate this, we use the **loss landscape visualisation** function of our package: We display this for the VGG-16 on CIFAR-100 in Figure 10. We see for the training loss 8a that the eigenvector corresponding to the largest eigenvalue $\lambda = 6.88$ only very locally corresponds to the sharpest increase in loss for the training, with other extremal eigenvectors, corresponding to the eigenvalues $\lambda = \{2.67, 2.35\}$ overtaking it in loss change relatively rapidly. Interestingly for the testing loss, all the extremal eigenvectors change the loss much more rapidly, contradicting previous assertions that the test loss is a "shifted" version of the training loss (He et al., 2019; Izmailov et al., 2018). We do however note some small asymmetry between the changes in loss along the opposite ends of the eigenvectors. The flat directions remain flat locally and some of the eigen-vectors corresponding to negative values correspond to decreases in test loss. To replicate this result, use the following command:

```

build_loss_landscape(
dataset='CIFAR100',
# dataset='CIFAR10', if testing on
CIFAR-10 data-set.
data_path='data/',
model='VGG16',
# Change accordingly for other
architectures such as PreResNet110
dist=0.25,
n_points=21,
spectrum_path='result/VGG16-CIFAR100/
spectra/spectrum-00300-ggn_lanczos'
,
# change accordingly for the Hessian
result
checkpoint_path='result/VGG16-CIFAR100/
checkpoint-00300.pt',
save_path='result/VGG16-CIFAR100/
losslandscape-00300.npz'
)

plot_loss_landscape('result/VGG16-CIFAR100/
losslandscape-00300.npz')
plt.show()

```

CIFAR-10 DATASET

To showcase the ability of our software to handle multiple datasets we display the Hessian of the VGG-16 trained in an identical fashion as its CIFAR-100 counterpart of CIFAR-10 in Figure 12, along with the a plot of a selection of Ritz vectors traversing the training loss surface in Figure 10a and testing loss surface in 10b along with also the training accuracy surface 11a and testing accuracy surface 11b

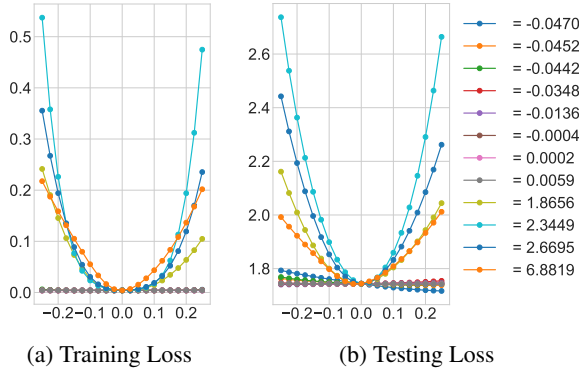


Figure 8. VGG-16 CIFAR-100 Loss surface visualised along 6 negative and position eigenvalues

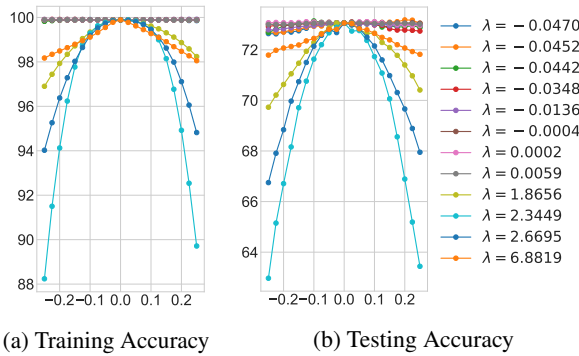


Figure 9. VGG-16 CIFAR-100 Accuracy surface visualised along 6 negative and position eigenvalues

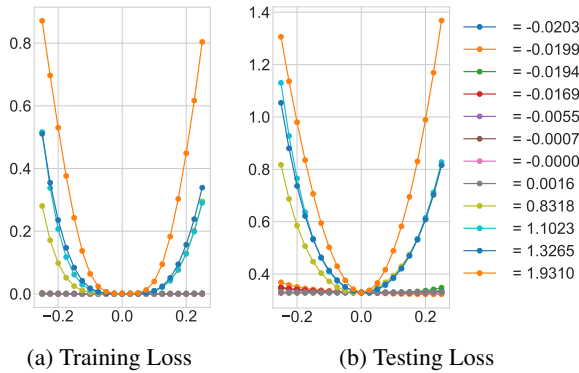


Figure 10. VGG-16 CIFAR-10 Loss surface visualised along 6 negative and position eigenvalues

7. Conclusion

We introduce **MLRG Deep Curvature** suite in **PyTorch** framework based on Lanczos algorithm that allows deep learning practitioners to learn spectral density information as well as eigenvalue/eigenvector pairs of the curvature matrices at specific points in weight space. Together with the software, we also include a succinct summary of the linear algebra, iterative method theory including proofs of conver-

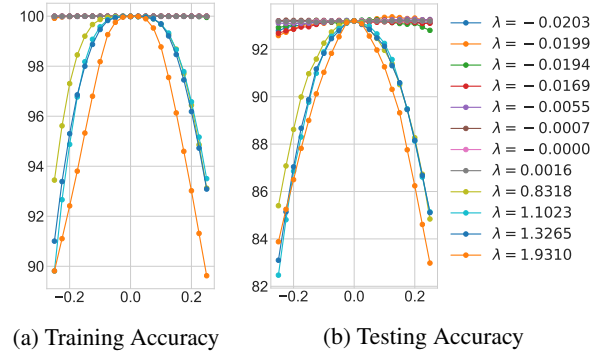


Figure 11. VGG-16 CIFAR-10 Accuracy surface visualised along negative and positive eigenvalues

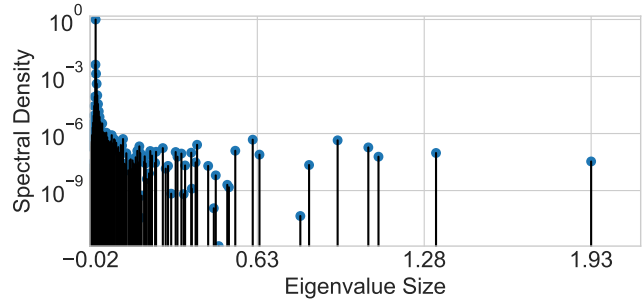


Figure 12. VGG-16 CIFAR-10 epoch 300 Hessian

gence and misconceptions and stochastic trace estimation that form the theoretical underpinnings of our work. Finally, we also included various examples of our package of analysis of both synthetic data and real data with modern neural network architectures.

References

Abadi, M., Barham, P., Chen, J., Chen, Z., Davis, A., Dean, J., Devin, M., Ghemawat, S., Irving, G., Isard, M., et al. TensorFlow: A system for large-scale machine learning. In *12th {USENIX} Symposium on Operating Systems Design and Implementation ({OSDI} 16)*, pp. 265–283, 2016.

Akemann, G., Baik, J., and Di Francesco, P. *The Oxford handbook of random matrix theory*. Oxford University Press, 2011.

Anonymous. Back{pack}: Packing more into backprop. In *Submitted to International Conference on Learning Representations, 2020a*. URL <https://openreview.net/forum?id=BJlrf24twB>. under review.

Anonymous. Towards understanding the true loss surface of deep neural networks using random matrix theory and iterative spectral methods. In *Submitted to*

- International Conference on Learning Representations*, 2020b. URL <https://openreview.net/forum?id=H1gza2NtWH>. under review.
- Bai, Z., Fahey, G., and Golub, G. Some large-scale matrix computation problems. *Journal of Computational and Applied Mathematics*, 74(1-2):71–89, 1996.
- Bishop, C. M. *Pattern recognition and machine learning*. springer, 2006.
- Chaudhari, P., Choromanska, A., Soatto, S., LeCun, Y., Baldassi, C., Borgs, C., Chayes, J., Sagun, L., and Zecchina, R. Entropy-SGD: Biasing gradient descent into wide valleys. *arXiv preprint arXiv:1611.01838*, 2016.
- Chollet, F. keras. <https://github.com/fchollet/keras>, 2015.
- Choromanska, A., Henaff, M., Mathieu, M., Arous, G. B., and LeCun, Y. The loss surfaces of multilayer networks. In *Artificial Intelligence and Statistics*, pp. 192–204, 2015a.
- Choromanska, A., LeCun, Y., and Arous, G. B. Open problem: The landscape of the loss surfaces of multilayer networks. In *Conference on Learning Theory*, pp. 1756–1760, 2015b.
- Chung, I.-H., Sainath, T. N., Ramabhadran, B., Picheny, M., Gunnel, J., Austel, V., Chauhari, U., and Kingsbury, B. Parallel deep neural network training for big data on blue gene/q. *IEEE Transactions on Parallel and Distributed Systems*, 28(6):1703–1714, 2017.
- Dauphin, Y. N., Pascanu, R., Gulcehre, C., Cho, K., Ganguli, S., and Bengio, Y. Identifying and attacking the saddle point problem in high-dimensional non-convex optimization. In *Advances in neural information processing systems*, pp. 2933–2941, 2014.
- Ghorbani, B., Krishnan, S., and Xiao, Y. An investigation into neural net optimization via Hessian eigenvalue density. *arXiv preprint arXiv:1901.10159*, 2019.
- Golub, G. H. and Meurant, G. Matrices, moments and quadrature. *Pitman Research Notes in Mathematics Series*, pp. 105–105, 1994.
- Golub, G. H. and Van Loan, C. F. *Matrix computations*, volume 3. JHU press, 2012.
- Graff, P., Feroz, F., Hobson, M. P., and Lasenby, A. Skynet: an efficient and robust neural network training tool for machine learning in astronomy. *Monthly Notices of the Royal Astronomical Society*, 441(2):1741–1759, 2014.
- Granziol, D. and Roberts, S. An Information and Field Theoretic approach to the Grand Canonical Ensemble, 2017.
- Granziol, D., Ru, B., Zohren, S., Dong, X., Osborne, M., and Roberts, S. Entropic spectral learning for large-scale graphs. *arXiv preprint arXiv:1804.06802*, 2018a.
- Granziol, D., Wagstaff, E., Ru, B. X., Osborne, M., and Roberts, S. Vbald-variational bayesian approximation of log determinants. *arXiv preprint arXiv:1802.08054*, 2018b.
- Granziol, D., Ru, B., Zohren, S., Dong, X., Osborne, M., and Roberts, S. Meme: An accurate maximum entropy method for efficient approximations in large-scale machine learning. *Entropy*, 21(6):551, 2019.
- He, H., Huang, G., and Yuan, Y. Asymmetric valleys: Beyond sharp and flat local minima. *arXiv preprint arXiv:1902.00744*, 2019.
- He, K., Zhang, X., Ren, S., and Sun, J. Deep residual learning for image recognition. In *Proceedings of the IEEE conference on computer vision and pattern recognition*, pp. 770–778, 2016.
- Hutchinson, M. F. A stochastic estimator of the trace of the influence matrix for Laplacian smoothing splines. *Communications in Statistics-Simulation and Computation*, 19(2):433–450, 1990.
- Ioffe, S. and Szegedy, C. Batch normalization: Accelerating deep network training by reducing internal covariate shift. *arXiv preprint arXiv:1502.03167*, 2015.
- Izmailov, P., Podoprikin, D., Garipov, T., Vetrov, D., and Wilson, A. G. Averaging weights leads to wider optima and better generalization. *arXiv preprint arXiv:1803.05407*, 2018.
- Kohler, J., Daneshmand, H., Lucchi, A., Zhou, M., Neymeyr, K., and Hofmann, T. Exponential convergence rates for batch normalization: The power of length-direction decoupling in non-convex optimization. *arXiv preprint arXiv:1805.10694*, 2018.
- Li, H., Xu, Z., Taylor, G., and Goldstein, T. Visualizing the loss landscape of neural nets. *arXiv preprint arXiv:1712.09913*, 2017.
- Lin, L., Saad, Y., and Yang, C. Approximating spectral densities of large matrices. *SIAM Review*, 58(1):34–65, 2016.
- Marchenko, V. A. and Pastur, L. A. Distribution of eigenvalues for some sets of random matrices. *Matematicheskii Sbornik*, 114(4):507–536, 1967.

- Martens, J. Deep learning via Hessian-free optimization. In *ICML*, volume 27, pp. 735–742, 2010.
- Martens, J. *Second-order optimization for neural networks*. PhD thesis, University of Toronto, 2016. URL http://www.cs.toronto.edu/~jmartens/docs/thesis_phd_martens.pdf.
- Martens, J. and Sutskever, I. Training deep and recurrent networks with Hessian-free optimization. In *Neural networks: Tricks of the trade*, pp. 479–535. Springer, 2012.
- Meurant, G. and Strakoš, Z. The Lanczos and conjugate gradient algorithms in finite precision arithmetic. *Acta Numerica*, 15:471–542, 2006.
- Nesterov, Y. *Introductory lectures on convex optimization: A basic course*, volume 87. Springer Science & Business Media, 2013.
- Papayan, V. The full spectrum of deep net Hessians at scale: Dynamics with sample size. *arXiv preprint arXiv:1811.07062*, 2018.
- Paszke, A., Gross, S., Chintala, S., Chanan, G., Yang, E., DeVito, Z., Lin, Z., Desmaison, A., Antiga, L., and Lerer, A. Automatic differentiation in Pytorch. 2017.
- Pearlmutter, B. A. Fast exact multiplication by the Hessian. *Neural computation*, 6(1):147–160, 1994.
- Pennington, J. and Bahri, Y. Geometry of neural network loss surfaces via random matrix theory. In *Proceedings of the 34th International Conference on Machine Learning-Volume 70*, pp. 2798–2806. JMLR. org, 2017.
- Roosta-Khorasani, F. and Ascher, U. Improved bounds on sample size for implicit matrix trace estimators. *Foundations of Computational Mathematics*, 15(5):1187–1212, 2015.
- Sagun, L., Bottou, L., and LeCun, Y. Eigenvalues of the Hessian in deep learning: Singularity and beyond. *arXiv preprint arXiv:1611.07476*, 2016.
- Sagun, L., Evci, U., Guney, V. U., Dauphin, Y., and Bottou, L. Empirical analysis of the Hessian of over-parametrized neural networks. *arXiv preprint arXiv:1706.04454*, 2017.
- Santurkar, S., Tsipras, D., Ilyas, A., and Madry, A. How does batch normalization help optimization? In *Advances in Neural Information Processing Systems*, pp. 2483–2493, 2018.
- Simonyan, K. and Zisserman, A. Very deep convolutional networks for large-scale image recognition. *arXiv preprint arXiv:1409.1556*, 2014.
- Tao, T. *Topics in random matrix theory*, volume 132. American Mathematical Soc., 2012.
- Ubaru, S. and Saad, Y. Applications of trace estimation techniques.
- Van Loan, C. F. and Golub, G. H. *Matrix computations*. Johns Hopkins University Press, 1983.
- Vinyals, O. and Povey, D. Krylov subspace descent for deep learning. In *Artificial Intelligence and Statistics*, pp. 1261–1268, 2012.
- Wigner, E. P. Characteristic vectors of bordered matrices with infinite dimensions i. In *The Collected Works of Eugene Paul Wigner*, pp. 524–540. Springer, 1993.

A. An Illustrated Example

We give an illustration on an example of using the MLRG-DeepCurvature package and more details, including detailed documentation of each user function and the output of this particular example, can be found at our open-source repository. We begin by importing the necessary functions and packages:

```
from core import *
from visualise import *
import matplotlib.pyplot as plt
```

In this example, we train a VGG16 network on CIFAR-100 for 100 epochs. In a test computer with AMD Ryzen 3700X CPU and NVIDIA GeForce RTX 2080 Ti GPU, each epoch of training takes less than 10 seconds:

```
train_network(
    dir='result/VGG16-CIFAR100/',
    dataset='CIFAR100',
    data_path='data/',
    epochs=100,
    model='VGG16',
    optimizer='SGD',
    optimizer_kwargs={
        'lr': 0.03,
        'momentum': 0.9,
        'weight_decay': 5e-4
    }
)
```

This step generates a number of training statistics files (starting with `stats-`) and checkpoint files (`checkpoint-00XXX.pt`, where `XXX` is the epoch number) that contain the `state_dict` of the optimizer and the model. We may additionally visualise the training processes by looking at the basic statistics by calling `plot_training` function. With the checkpoints generated, we may now compute analyse the eigenspectrum of the curvature matrix evaluated at the desired point of training. For example, if we would like to evaluate the Generalised Gauss-Newton (GGN) matrix at the end of the training with 20 Lanczos iterations, we call:

```
compute_eigenspectrum(
    dataset='CIFAR100',
    data_path='data/',
    model='VGG16',
    checkpoint_path='result/VGG16-CIFAR100/
        checkpoint-00100.pt',
    save_spectrum_path='result/VGG16-
        CIFAR100/spectra/spectrum-00100-
        ggn_lanczos',
    save_eigvec=True,
    lanczos_iters=20,
    curvature_matrix='ggn_lanczos',
)
```

This function call saves the spectrum results (including eigenvalues, eigenvectors and other related statistics) in the

`save_spectrum_path` path string defined. To visualise the spectrum as stem plot similar to Figure 6, we simply call:

```
plot_spectrum('lanczos', path='result/VGG16-
    CIFAR100/spectra/spectrum-00100-
    ggn_lanczos.npz')
plt.show()
```

Finally, with the eigenvalues and eigenvectors computed, we might be interested in knowing how sensitive the network is to perturbation along these directions. To achieve this, we first construct a loss landscape by setting the number of query points and maximum perturbation to apply. To achieve that, we call:

```
build_loss_landscape(
    dataset='CIFAR100',
    data_path='data/',
    model='VGG16',
    dist=1.,
    n_points=21,
    spectrum_path='result/VGG16-CIFAR100/
        spectra/spectrum-00100-ggn_lanczos',
    checkpoint_path='result/VGG16-CIFAR100/
        checkpoint-00100.pt',
    save_path='result/VGG16-CIFAR100/
        losslandscape-00100.npz'
)

plot_loss_landscape('result/VGG16-CIFAR100/
    losslandscape-00100.npz')
plt.show()
```

where in this example, we set the maximum perturbation to be 1 (`dist` argument) and number of query points along each direction to be 21 (`n_points` argument). This will produce diagrams similar to Figure 10 that show the effect of perturbation in the loss and accuracy for both training and testing.